

Distinguishing nuclei-specific benzo[*a*]pyrene-induced effects from whole-cell alterations in MCF-7 cells using Fourier-transform infrared spectroscopy

Blessing E. Obinaju¹, Nigel J. Fullwood² and Francis L. Martin^{1,*}

¹*Centre for Biophotonics, Lancaster Environment Centre, Lancaster University, Bailrigg, Lancaster LA1 4YQ, UK;* ²*Division of Biomedical and Life Sciences, Faculty of Health and Medicine, Lancaster University, UK*

Corresponding author: Prof Francis L Martin PhD, Centre for Biophotonics, LEC, Lancaster University, Lancaster LA1 4YQ, UK; Tel.: +44(0)1524 510206; Email: f.martin@lancaster.ac.uk

Abstract

Exposure to chemicals such as benzo[*a*]pyrene (B[*a*]P) can generate intracellular toxic mechanisms. Fourier-transform infrared (FTIR) spectroscopy is a novel approach that allows the non-destructive analysis of underlying chemical bond alterations in patho-physiological processes. This study set out to examine whether B[*a*]P-induced whole cell alterations could be distinguished from effects on nuclei of exposed cells. Using attenuated total reflection FTIR (ATR-FTIR) spectroscopy, alterations in nuclei isolated from B[*a*]P-treated MCF-7 cells concentrated either in G₀/G₁- or S-phase were observed. B[*a*]P-induced effects in whole-cells included alterations to lipids, DNA and protein spectral regions. Absorbance areas for protein and DNA/RNA regions in B[*a*]P-treated whole cells differed significantly ($P < 0.0001$) from vehicle controls and these observations correlated with alterations noted in isolated nuclei. Our findings provide evidence that FTIR spectroscopy has the ability to identify specific chemical-induced alterations.

Keywords: ATR-FTIR spectroscopy; Benzo[*a*]pyrene; DNA damage; MCF-7 cells; nucleus isolation; Polycyclic aromatic hydrocarbon

1. Introduction

Benzo[*a*]pyrene (B[*a*]P) is a polycyclic aromatic hydrocarbon (PAH), capable of inducing genotoxic events in biological organisms. In mammalian cells, B[*a*]P is effectively metabolised (Arlt et al., 2008), a process which facilitates B[*a*]P-induced toxicity in cells through: **1)** DNA modification *via* covalent binding of reactive metabolites [BaP-7,8-diol-9,10-epoxide (BPDE)] to bases, *e.g.*, guanine or adenine (Phillips, 1983); and, **2)** binding to aryl hydrocarbon (AHR) receptor. The AHR is a cytosolic ligand-activated transcription factor responsible for sensing extracellular signals and environmental stresses affecting cell growth and development (Hamouchene et al., 2011). Thus, high-affinity AHR ligands, *e.g.*, B[*a*]P and other PAHs, are capable of altering cell cycle processes including G₀/G₁-phase arrest or its evasion (Khan and Dipple, 2000). Cells at various stages in their cycle have been shown to respond differently to chemical exposures, especially to B[*a*]P (Hamouchene et al., 2011; Pang et al., 2012). These observations are significant towards understanding changes occurring in specific cell populations (*e.g.*, neurons *vs* epithelial cells).

Infrared (IR) spectroscopy, including techniques such as Fourier-transform IR (FTIR) spectroscopy, has enhanced the study of cells and cell cycle processes, including observations at subcellular levels (Hammiche et al., 2005; Pang et al., 2012; Pijanka et al., 2009). Such biospectroscopy techniques provide a rapid, as well as a direct, alternative approach for analysing the cell, and a sensitive, reagent-free method for detecting intracellular changes, including within its subcellular components (Lipiec et al., 2014). The ability to detect slight changes in the IR spectra of samples at wavenumbers representative of biomolecules, *e.g.*, symmetric (1088 cm⁻¹) and asymmetric (1234 cm⁻¹) PO₂⁻ bands, which typically can be associated with nucleic acids, are significant for understanding the differences between normal and malignant conditions (Lasch et al., 2002). More importantly, the potential to rapidly study isolated cell components, *e.g.*, nucleus (Holton et al., 2011; Lasch et al., 2002;

Lipiec et al., 2014; Pijanka et al., 2009), and the primary contents of the nucleus in biological cells (DNA or RNA) (Banyay et al., 2003; Dovbeshko et al., 2000) is a significant advantage. Using this technique, it is possible to derive a chemical signature of a disease process by directly comparing acquired spectroscopic data from differing biological states because, IR spectra are a holistic reflection of the chemical composition of interrogated samples (Holton et al., 2011). The optimization of biospectroscopy protocols greatly increases the sensitivity and resolution of IR spectroscopy and expands its application (Baker et al., 2014; Obinaju and Martin, 2013; Obinaju et al., 2014).

Using FTIR coupled to an attenuated total reflection (ATR) attachment, this study investigated the human mammary carcinoma (MCF-7) cell line in quiescent (G_0/G_1 -phase) and exponential (S-phase) growth phases of the cell cycle, comparing induced alterations in whole cells and isolated nuclei of B[a]P-treated cells. The rationale of the study was to determine whether biospectroscopy approaches can identify underlying sub-cellular alterations even within the milieu of the whole cell.

2. Materials and Methods

2.1 Cell culture

The MCF-7 cell line was grown in Dulbecco's modified essential medium (DMEM) supplemented with 10% heat-inactivated foetal calf serum, 100 U/ml penicillin and 100 μ g/ml streptomycin. MCF-7 cells were cultured routinely in 75 cm² flasks at 5% CO₂ in air and 37°C in a humidified atmosphere and sub-cultured (1:10 v/v) twice weekly. Prior to incorporation into experiments, cultured cells were disaggregated using 5 ml of a 0.05% trypsin solution for 5 min, to form single cell suspensions. Trypsin was inactivated using 5 ml of complete DMEM and cells were centrifuged at 120 g for 5 min. Cell pellets were re-suspended in 10 ml of complete DMEM and 1 ml cell aliquots were seeded into 25 cm²

flasks. The cells were concentrated in G₀/G₁-phase (96-h incubation) or S-phase (24-h incubation) growth phase, as previously described (Jiao et al., 2007). Cells were treated with 10⁻⁹ or 10⁻⁶ M B[a]P using dimethyl sulfoxide (DMSO) as vehicle control (≤1% v/v). Growth medium was replaced with fresh DMEM for G₀/G₁-phase cells, 5 h prior to treatment with test agent. Treatments were for 24 h, after which cells were trypsin-disaggregated and single cell suspensions were fixed in 70% ethanol, pipetted onto IR-reflective Low-E glass slides (Kevley Technologies, Chesterland, OH, USA), air-dried, desiccated and interrogated using ATR-FTIR spectroscopy. All experiments were conducted in triplicate and data presented was obtained from three independent experiments.

2.2 Nuclei Isolation

MCF-7 cell nuclei were isolated using the Nuclei EZ prep nuclei isolation kit (Sigma, UK) protocol for suspension cell lines. Briefly, following 24-h treatment with test agent, cells were trypsin-disaggregated and washed in ice-cold phosphate buffered saline (PBS). Cells were completely lysed in 2 ml ice-cold Nuclei EZ lysis buffer by vortexing briefly at high speed and set on ice for 45 min, then vortexing every 10 min. Isolated nuclei pellets were collected by centrifugation at 500 g for 5 min at 4°C. Nuclei purification was done by washing pellets in 2 ml of ice-cold Nuclei EZ lysis buffer, vortexing briefly at high speed and placing on ice for 5 min. Purified nuclei pellets were collected by centrifugation (500 g for 5 min at 4°C), fixed in 70% ethanol, pipetted onto IR-reflective Low-E slides and desiccated.

2.3 Scanning electron microscopy (SEM)

Ethanol-fixed MCF-7 cells or isolated nuclei pellets were mounted on aluminium specimen stubs, air-dried and sputter-coated with gold (Au) using an Edwards S150A sputter coater and examined on a JEOL J.S.M 5600 scanning electron microscope.

2.4 Data acquisition and spectra processing

Spectra was acquired using a Bruker TENSOR 27 FTIR spectrometer with Helios ATR attachment (Bruker Optics Ltd., Coventry, UK) containing a diamond crystal ($\sim 250 \mu\text{m} \times 250 \mu\text{m}$ sampling area). For each experimental condition (*i.e.*, sample slide), 10 spectra were acquired randomly from 10 independent areas of the slide [total 540 spectra = 10 spectra \times 3 slides per treatment/experiment \times 3 treatments \times 3 experiments \times 2 observations (intact cell vs. nuclei)]. The ATR crystal was cleaned with dH_2O , dried thoroughly and a new background spectrum taken prior to the interrogation of each sample slide. Raw spectra acquired in the $4000 \text{ cm}^{-1} - 400 \text{ cm}^{-1}$ range (3.84 cm^{-1} spectral resolution with 32 co-additions) from the interrogated samples were pre-processed prior to computational analysis. Spectra were cut to the region of interest (biochemical cell fingerprint: $1800 \text{ cm}^{-1} - 900 \text{ cm}^{-1}$), baseline-corrected and normalized to the Amide I peak (1650 cm^{-1}). Normalized spectra were mean-centred prior to the application of multivariate analysis [principal component analysis and linear discriminant analysis (PCA-LDA)], where PCA was used for preliminary data reduction and LDA derived vectors from principal components (PCs), minimizing intra-category variance and maximizing inter- category variance (Martin et al., 2007). Multivariate analysis results were viewed either as scores plots or cluster vectors plots. For each cluster vectors plot generated, the toolbox used was set to identify the top six wavenumbers responsible for the variance between the treatment categories (Trevisan et al., 2010). Pre-processing and computational analysis were performed in MATLAB R2011b (The Mathworks Inc., USA), using an in-house developed IRTools toolbox available at <http://trevisanj.github.io/irootlab/> (Trevisan et al., 2013).

2.5 Statistical analysis

The Mann-Whitney *U*-test, one-way analysis of variance (*ANOVA*) and the Dunnett's multiple comparison tests were used to determine statistical significance between treated-cell populations and corresponding controls. Linear regression and Pearson correlations were used to determine relationships between variables.

3. Results

3.1 SEM

Photomicrographs show the presence of nuclei in control MCF-7 cells (Fig. 1A). Upon isolation, nuclei from both the vehicle control fraction (Fig. 1B) and the 10^{-9} M B[a]P-treated nuclei fraction (Fig. 1C) appeared similar and of a relatively consistent structure, although the latter appear mildly distorted. However, 10^{-6} M B[a]P-treated nuclei showed signs of deformity, even after just 24-h exposure (Fig. 1D).

3.2 Multivariate analysis

In a PCA-LDA scores plot [see Electronic Supplementary Information (ESI) Fig. S1], treated whole-cell or isolated nuclei MCF-7 cell populations in G_0/G_1 -phase exhibit a dose-related response and a positive index along the first linear discriminant (LD1) space. In S-phase, high concentrations of B[a]P (10^{-6} M) generated a negative index in LD1 for both whole-cell and isolated nuclei. The observed MCF-7 cell responses to B[a]P treatment were significantly ($P < 0.0001$) different from each other as determined using *ANOVA* and treated-cell populations were significantly different from control as determined using Dunnett's multiple comparison tests ($P < 0.05$). Distinguishing wavenumbers for intact cell and isolated nuclei for G_0/G_1 - (Table 1) and S-phase (Table 2) show the spectral biomarkers following exposure.

PCA-LDA derived cluster vectors plots comparing treated-cell populations to vehicle control (Figs. 2 and 3) in whole cells and isolated nuclei, show B[a]P-induced alterations associated with distinguishing wavenumbers. Wavenumbers distinguishing whole cells from nuclei included 1207 cm^{-1} and 964 cm^{-1} (G_0/G_1 -phase) and 1647 cm^{-1} (S-phase). Nuclei were distinguished from whole cells by wavenumbers 1713 cm^{-1} and 964 cm^{-1} in vehicle control cells, irrespective of G_0/G_1 - or S-phase. Results show that B[a]P induced marked dose-related alterations in the DNA/RNA ($\sim 1260\text{ cm}^{-1} - 990\text{ cm}^{-1}$) region of the biochemical-cell fingerprint in whole-cell populations in both phases of the cell cycle; 10^{-6} M B[a]P induced changes to the lipid region (1744 cm^{-1} , 1740 cm^{-1}) in isolated nuclei (Fig 2).

Using the mean absorbance band areas for nucleic acids ($1000 - 1140\text{ cm}^{-1}$), Amide II ($1478 - 1580\text{ cm}^{-1}$), protein phosphorylation ($980 - 780\text{ cm}^{-1}$) and lipids ($2923 - 2852\text{ cm}^{-1}$), the nucleic acid-to-protein ratio, lipid-to-phosphorylated protein ratio and the lipid-to-nucleic acid ratio were calculated for cells in both cell cycle phases (Fig. 4), as a possible measure of apoptosis signalling in response to B[a]P-induced DNA damage in MCF-7 cells (Gasparri and Muzio, 2003; Liu et al., 2001). Results show an inverse relationship between nucleic acid/protein and treatment concentrations (Figs. 4 and 5). To assess the relationship between B[a]P-induced alterations in whole cell to the alterations within the nucleus, the mean peak areas of absorbance corresponding to Amide I ($1704 - 1589\text{ cm}^{-1}$), Amide II ($1580 - 1478\text{ cm}^{-1}$), RNA/DNA ($1140 - 1000\text{ cm}^{-1}$) and protein phosphorylation ($980 - 780\text{ cm}^{-1}$) in isolated nuclei and whole cells were plotted against each other (Fig. 5). A significant ($P < 0.0001$) and strong positive correlation was observed in G_0/G_1 -phase ($r^2 = 0.991$) and S-phase ($r^2 = 0.992$). At 10^{-6} M B[a]P concentrations a significant decrease in concentrations of nucleic acids ($P < 0.0001$) was induced, with a significant increase in proteins ($P < 0.05$) in both growth phases of the cell cycle and a significant increase in lipids ($P < 0.001$) in S-phase (see ESI Table S1).

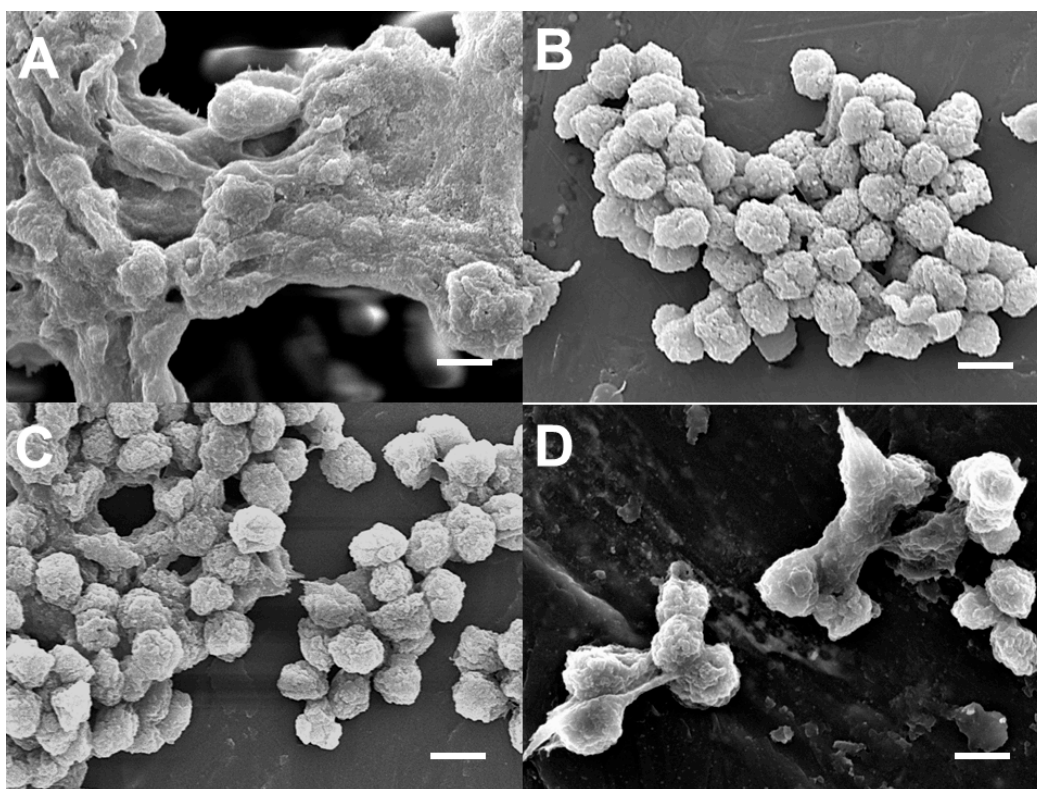


Fig. 1 SEM photomicrographs of (A) Intact and untreated MCF-7 cells compared to isolated nuclei pellets from: (B) DMSO-treated (vehicle control); (C) 10^{-9} M B[a]P-treated; and, (D) 10^{-6} M B[a]P-treated MCF-7 cells. Note the 10^{-6} M B[a]P-treated cells (D) are heavily distorted compared to the control (B) whilst the 10^{-9} M B[a]P-treated cells (C) show evidence of a small amount of distortion. Scale bars = 5 microns

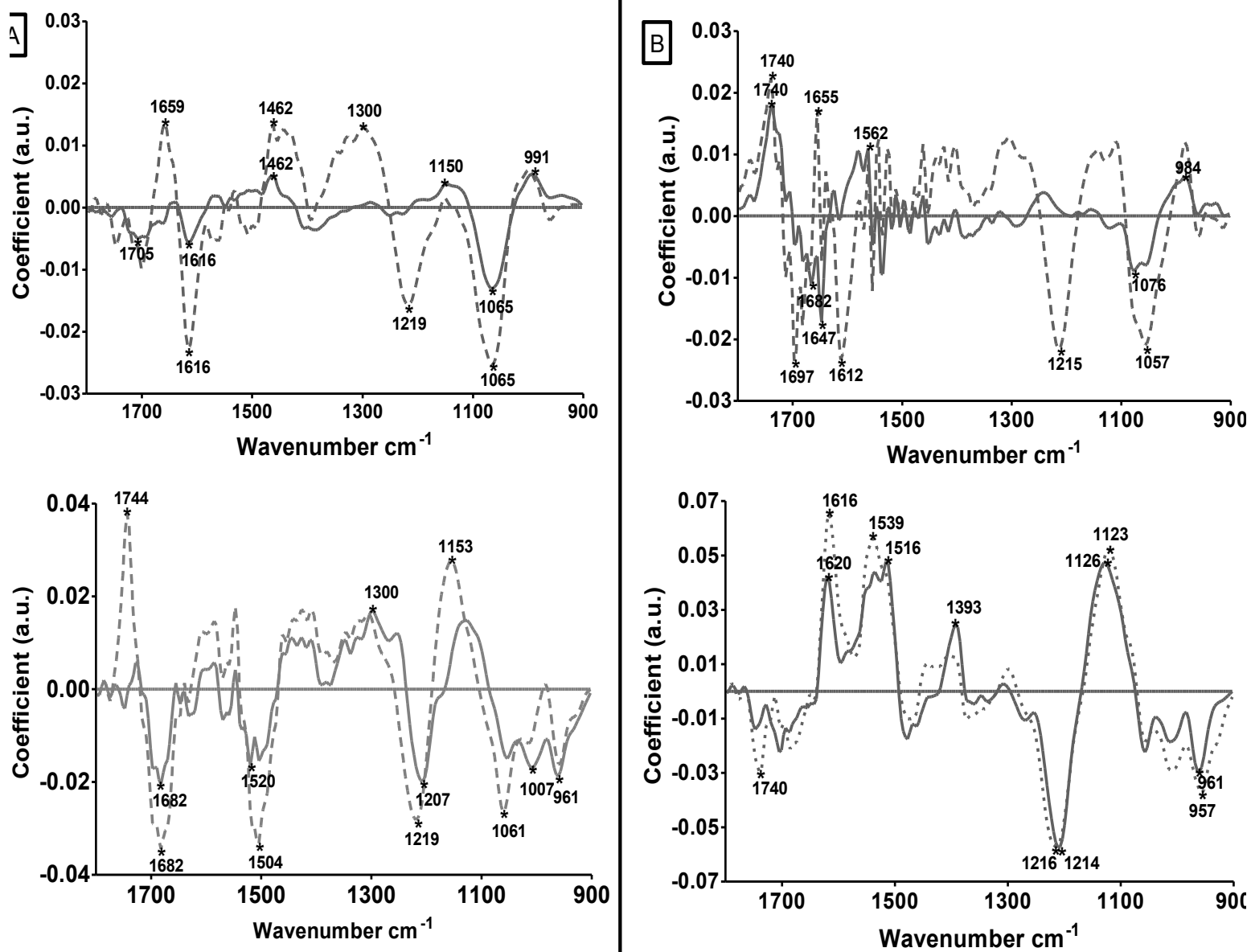


Fig. 2 Cluster vectors plots comparing vehicle control (line at origin), 10^{-9} M (solid lines) and 10^{-6} M (broken lines) of B[a]P-treated MCF-7 cells concentrated in G_0/G_1 -phase (A) or S-phase (B): whole-cells (top panels) or isolated nuclei (lower panels). Spectra were cut between $1800 - 900 \text{ cm}^{-1}$, baseline-corrected and normalized to the Amide I peak (1650 cm^{-1}). Normalized spectra were mean-centred prior to PCA-LDA. Plots were generated following PCA-LDA and show top six discriminating wavenumbers.

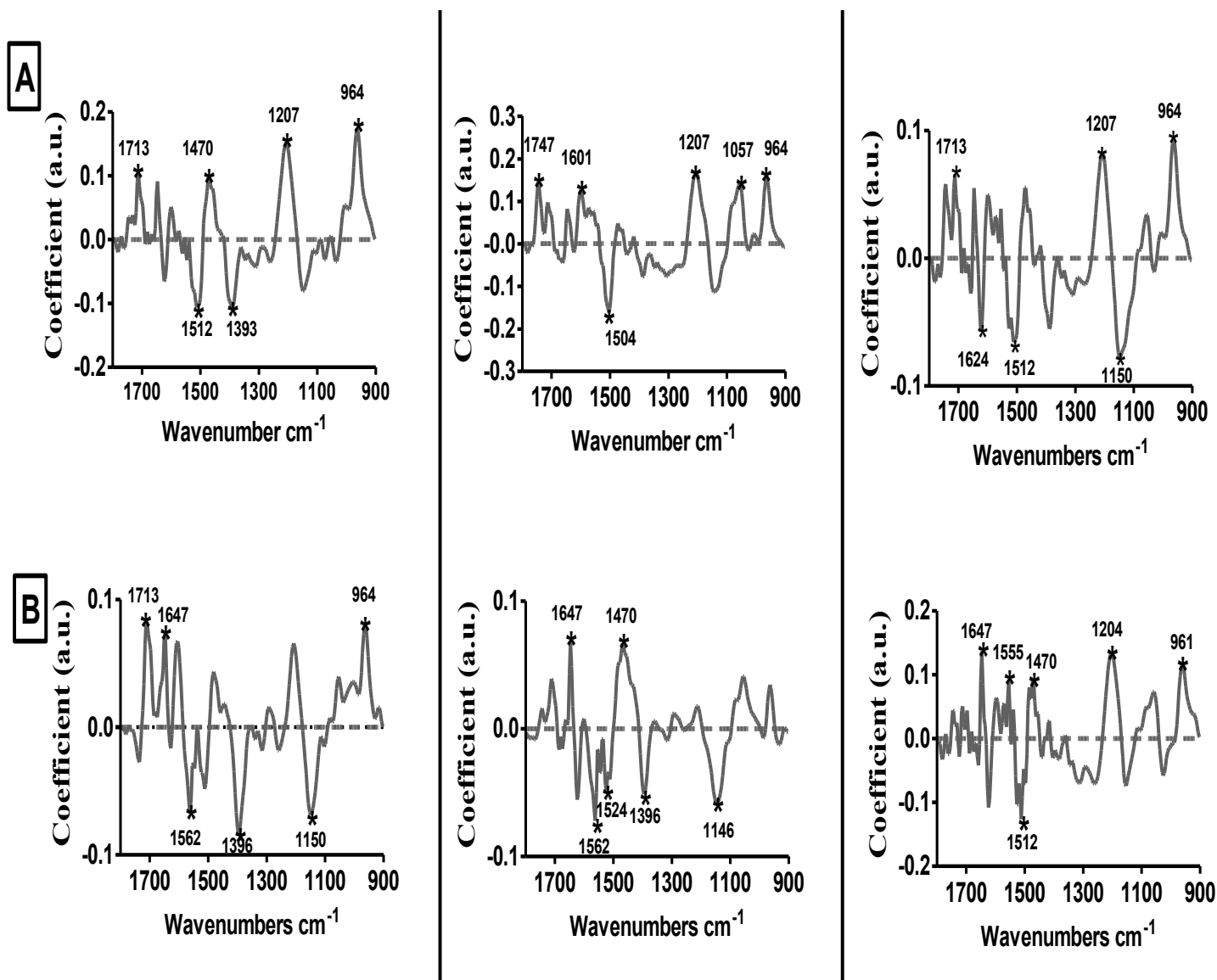


Fig. 3 Cluster vectors plots comparing various categories of whole-cell (broken lines) and isolated nuclei (solid lines) of G_0/G_1 -phase (**A**) or S-phase (**B**) B[a]P-treated MCF-7 cells; vehicle control (left column); 10^{-9} M (middle column) and 10^{-6} M (right column). Spectra were cut between $1800 - 900 \text{ cm}^{-1}$, baseline-corrected and normalized to the Amide I peak (1650 cm^{-1}). Normalized spectra were mean-centred; plots were obtained following PCA-LDA and show top six discriminating wavenumbers.

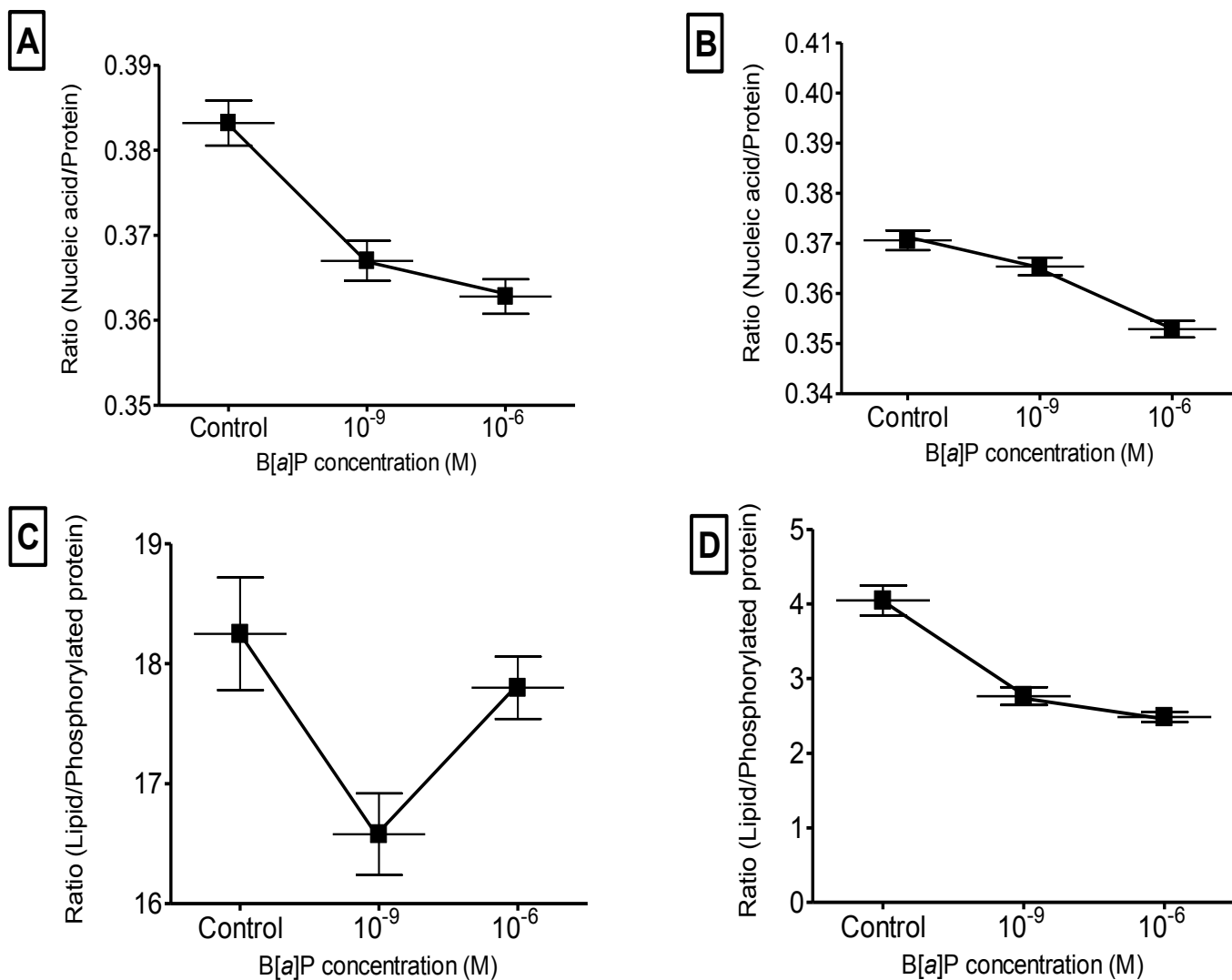


Fig. 4 Nucleic acid-to-protein ratio (**A & B**) and lipid-to-phosphorylated protein ratio (**C & D**) for benzo[*a*]pyrene (B[*a*]P)-treated MCF-7 cells in G₀/G₁- (**A & C**) or S-phase (**B & D**). The values are mean ± SEM peak areas for absorbance at Amide II (1580 - 1478 cm⁻¹), nucleic acid (1140 - 1000 cm⁻¹), lipids (2932 - 2852 cm⁻¹) and protein phosphorylation (980 - 780 cm⁻¹) in infrared spectra acquired from three independent experiments.

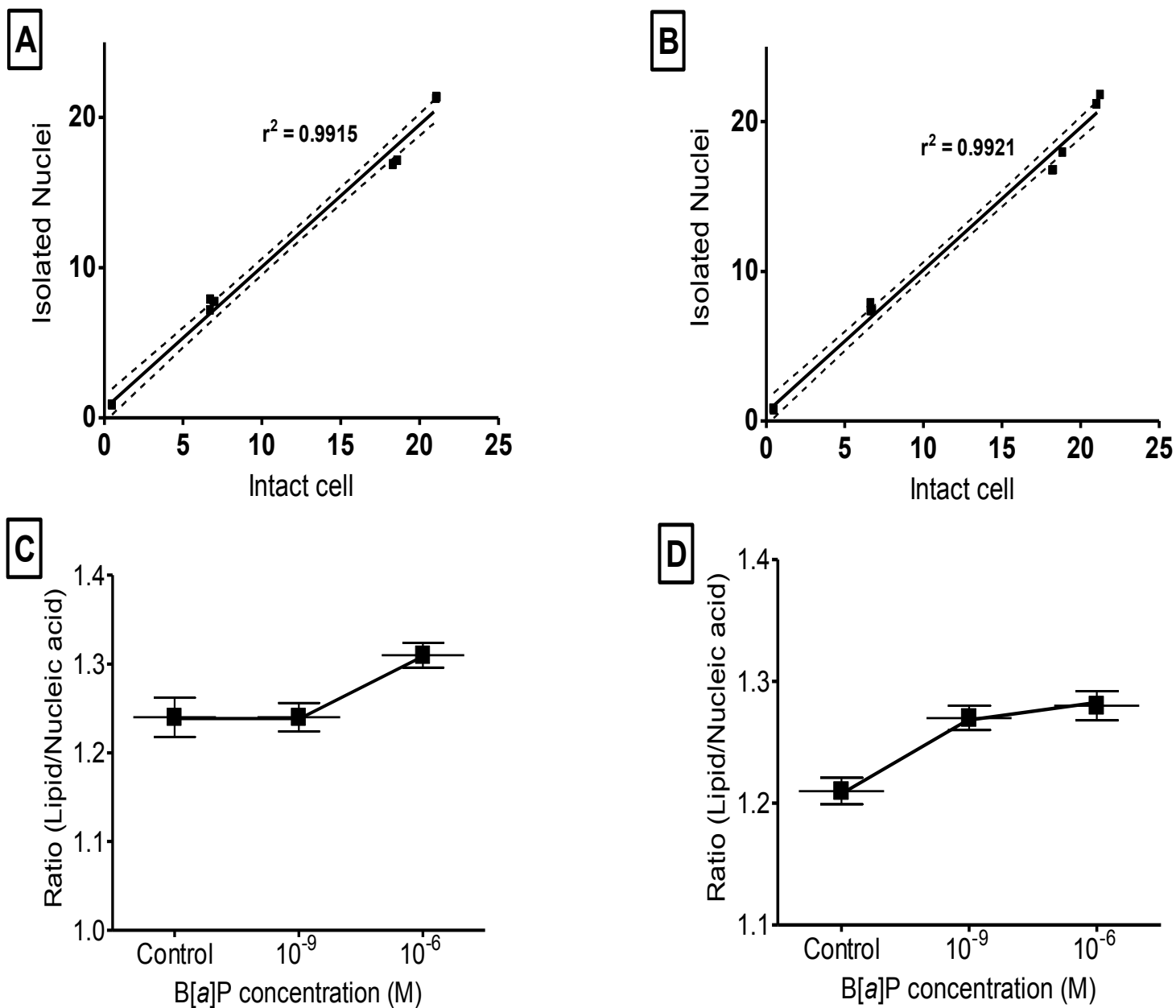


Fig. 5 Linear relationship between alterations in whole cells to alterations in isolated nuclei (**A & B**) and the lipid-to-nucleic acid ratio (**C & D**) for benzo[*a*]pyrene (B[*a*]P)-treated MCF-7 cells in G_0/G_1 - (**A & C**) or S-phase (**B & D**) of the cell cycle. Values are the mean (**A & B**) or mean \pm SEM (**C & D**) peak areas for absorbance at Amide I ($1704 - 1589 \text{ cm}^{-1}$), Amide II ($1580 - 1478 \text{ cm}^{-1}$), nucleic acids ($1140 - 1000 \text{ cm}^{-1}$) and protein phosphorylation ($980 - 780 \text{ cm}^{-1}$) in (**A & B**) and lipids ($2932 - 2852 \text{ cm}^{-1}$) / nucleic acids ($1140 - 1000 \text{ cm}^{-1}$) in (**C & D**). Infrared spectra were acquired from three independent experiments.

Table 1 Attenuated total reflection Fourier-transform infrared (ATR-FTIR) spectroscopy distinguishing wavenumbers as shown in cluster vectors plots and corresponding tentative chemical assignments: wavenumbers responsible for variance between vehicle control and treatment groups in whole cells and isolated nuclei of benzo[*a*]pyrene-treated MCF-7 cells in G₀/G₁-phase.

| Sample | Treatment | Distinguishing wavenumbers (cm ⁻¹) | Tentative assignments | References |
|-----------------|-----------------------------------|--|--|------------|
| Whole cell | 10 ⁻⁹ M B[<i>a</i>]P | 1705 | Fatty acid esters | 1 |
| | | 1616 | Amide I (Carbonyl stretching vibrations in side chains of amino acids) | 3 |
| | | 1462 | | |
| | | 1150 | C-O stretching of carbohydrates | 1 |
| | | 1065 | C-O stretching of phosphodiester bonds and ribose | 1 |
| | | 991 | C-O stretching in ribose | 1 |
| | 10 ⁻⁶ M B[<i>a</i>]P | 1659 | Amide I | 1 |
| | | 1616 | Amide I (Carbonyl stretching vibrations in side chains of amino acids) | 3 |
| | | 1462 | CH ₂ bending of lipids | 3 |
| | | 1300 | Amide III | 1 |
| | | 1219 | PO ₂ ⁻ asymmetric stretching vibrations of nucleic acids | 1 |
| | | 1065 | C-O stretching of phosphodiester bonds and ribose | 1 |
| Isolated Nuclei | 10 ⁻⁹ M B[<i>a</i>]P | 1682 | C=O guanine deformation | 1 |
| | | 1520 | Purinic and Pyrimidinic vibrations | 2 |
| | | 1300 | Vibrational coupling between a base and a sugar | 2 |
| | | 1207 | PO ₂ ⁻ asymmetric (Phosphate I) stretching vibrations | 1 |
| | | 1007 | C-O stretching in deoxyribose | 1 |
| | | 961 | C-O deoxyribose | 1 |
| | 10 ⁻⁶ M B[<i>a</i>]P | 1744 | Lipids (possibly nuclear lipids) | |
| | | 1682 | C=O guanine deformation | 1 |
| | | 1504 | Purinic and Pyrimidinic vibrations | 2 |
| | | 1219 | PO ₂ ⁻ asymmetric stretching vibrations of nucleic acid when highly hydrogen bonded; RNA C-H ring bending | 1, 2 |
| | | 1153 | Stretching vibrations of hydrogen bonding in C-OH groups | 1 |
| | | 1061 | C-O stretching in deoxyribose / one of the triad peaks of nucleic acid (along with 1031 and 1081 cm ⁻¹); Ribose C-O stretching | 1, 2 |

- References: (1) Movasaghi et al. (2008); (2) Stuart (2005); (3) Obinaju et al. (2014)

Table 2 Attenuated total reflection Fourier-transform infrared (ATR-FTIR) spectroscopy distinguishing wavenumbers as shown in cluster vectors plots and corresponding tentative chemical assignments: wavenumbers responsible for variance between vehicle control and treatment groups in whole cells and isolated nuclei of benzo[*a*]pyrene-treated MCF-7 cells in S-phase.

| Sample | Treatment | Distinguishing wavenumbers (cm ⁻¹) | Tentative assignments | References |
|-----------------|-----------------------------------|--|---|------------|
| Intact cell | 10 ⁻⁹ M B[<i>a</i>]P | 1740 | C=O stretching (Lipids) | 1 |
| | | 1682 | Unordered random coils and turns of Amide I | 1 |
| | | 1647 | Amide I | 1 |
| | | 1562 | CO stretching predominantly α -sheet of Amide II | 1,3 |
| | | 1076 | Symmetric phosphate stretching vibrations | |
| | | 984 | OCH ₃ (polysaccharides - cellulose) | |
| | 10 ⁻⁶ M B[<i>a</i>]P | 1740 | C=O stretching (Lipids) | 1 |
| | | 1697 | A high frequency vibration of an antiparallel β -sheet of Amide I | 1 |
| | | 1655 | Amide I (of proteins in α -helix conformation), | 1, 3 |
| | | 1612 | Amide I (Carbonyl stretching vibrations in side chains of amino acids) | 3 |
| | | 1215 | Amide III | 3 |
| | | 1057 | Stretching C-O deoxyribose | 1 |
| Isolated Nuclei | 10 ⁻⁹ M B[<i>a</i>]P | 1620 | Peak of nucleic acids due to base carbonyl stretching and ring breathing mode | 1 |
| | | 1516 | Purinic and Pyrimidinic vibrations | 2 |
| | | 1393 | Vibrational coupling between a base and a sugar | 2 |
| | | 1214 | PO ₂ ⁻ asymmetric (Phosphate I) stretching vibrations | 1 |
| | | 1126 | Sugar - phosphate chain vibrations | 2 |
| | | 961 | C-O deoxyribose | 1 |
| | 10 ⁻⁶ M B[<i>a</i>]P | 1740 | Lipids (possibly nuclear lipids) | |
| | | 1616 | Purinic and Pyrimidinic vibrations, DNA C=O stretching; N-H bending; RNA C=O stretching | 2 |
| | | 1539 | Purinic and Pyrimidinic vibrations | 2 |
| | | 1216 | RNA C-H ring bending | 2 |
| | | 1123 | RNA ribose C-O stretching | 2 |
| | | 957 | sugar/sugar - phosphate vibrations | 1 |

- References: (1) Movasaghi et al. (2008); (2) Stuart (2005); (3) Obinaju et al. (2014)

4. Discussion

PAHs, such as B[a]P, are metabolically biotransformed in organisms. This metabolic process can generate reactive intermediates, which alter the structure of DNA molecules by covalent binding (Malins et al., 2006). This might explain the deformity of isolated nuclei at the highest dose of B[a]P used in this study (Fig. 1D). For instance, induction of apoptosis following exposure to toxic chemicals could explain such nuclei deformity (nuclear and cytoplasmic shrinkage, chromatin condensation, inter-nucleosomal DNA cleavage and plasma membrane blebbing) (Zelig et al., 2009).

Cellular responses to B[a]P exposure is time, concentration and cell type dependent (Hockley et al., 2006; Pang et al., 2012). A positive trend observed in treated cells (see ESI Fig. S1) suggests an increase in total biomolecules (Llabjani et al., 2014). The positive index observed in treated cells may well be a result of B[a]P-induced cell proliferation. B[a]P, as well as its metabolites, has been shown to be mitogenic in human mammary epithelial cell cultures (Tannheimer et al., 1997; 1998), possibly by activating the epidermal growth factor receptor (EGFR) signalling pathway in the cells and altering cell cycle processes, such as G₀/G₁-phase arrest (Khan and Dipple, 2000).

Wavenumbers within the biochemical-cell fingerprint (1800 - 900 cm⁻¹) provide information on particular molecules, *e.g.*, lipids (~1750 cm⁻¹). The intensity, area and centroid position of the absorption bands are dependent on the concentration and structure of the absorbing molecule (Cakmak et al., 2006; Obinaju et al., 2015; Severcan et al., 2005). Thus, it is possible to detect treatment-altered biomolecules based on increased/decreased intensity levels, changes to area of absorption bands, and shifts in the centroid position of absorption bands. The marked changes to B[a]P-treated cells, especially changes within the DNA/RNA region comprising Amide III (~1260 cm⁻¹), asymmetric phosphate stretching

vibrations ($\nu_{\text{as}}\text{PO}_2^-$; $\sim 1225\text{ cm}^{-1}$), carbohydrate ($\sim 1155\text{ cm}^{-1}$), symmetric phosphate stretching vibrations ($\nu_{\text{s}}\text{PO}_2^-$; $\sim 1080\text{ cm}^{-1}$), glycogen ($\sim 1030\text{ cm}^{-1}$) and phosphorylated protein ($\sim 970\text{ cm}^{-1}$) peaks is expected. This observation is in agreement with documented observations in quiescent vs. exponential growth phase MCF-7 cells (Pang et al., 2012).

Base pairing between complementary strands and stacking between adjacent bases are the two factors mainly responsible for the stability of the DNA double helix (Yakovchuk et al., 2006). Within the nucleus, bands between 1800 cm^{-1} and 1500 cm^{-1} are considered sensitive markers for base pairing and base stacking effects in nucleic acids and originate from nucleobase vibrations (Banyay et al., 2003; Stuart, 2005). As observed in isolated nuclei, the band at 1713 cm^{-1} is the C=O stretching mode caused by base pairing in nucleic acids (Lipiec et al., 2014). The IR band at 964 cm^{-1} is due to C–C, C–O stretching of deoxyribose in the DNA backbone (Banyay et al., 2003; Movasaghi et al., 2008) and that at 1647 cm^{-1} is assigned to single-stranded cytosine in nucleic acids (Banyay et al., 2003). B[a]P-induced alterations in nuclei of G₀/G₁- and S-phase cells occurring within $1800 - 1500\text{ cm}^{-1}$ region (Fig. 2), are possibly changes to DNA structural conformation due to covalent binding to nucleic acid bases, *i.e.*, guanine or disruption of base pairing and base stacking interactions. Alterations to phosphate groups ($\nu_{\text{as}}\text{PO}_2^-$, Phosphate I and $\nu_{\text{s}}\text{PO}_2^-$, Phosphate II) (Tables 1 & 2) are possibly connected with spatial changes in the position of phosphate groups of nucleic acids (Dovbeshko et al., 2000).

The nucleus of eukaryotic cells is known to contain lipids, specifically phospholipids such as phosphatidylcholine (Irvine, 2003). These are thought to play a role in proliferation, differentiation and apoptotic processes (Ledeen and Wu, 2006). Alterations associated with 1744 cm^{-1} and 1740 cm^{-1} in isolated nuclei induced at the highest B[a]P concentration, may be indicative of induction of the apoptotic pathway, *i.e.*, the externalization of

phosphatidylserine (Balasubramanian et al., 2007). Compared to control cell populations, changes to nuclei lipids in the biofingerprint spectral region may be an IR biomarker of chemical-induced necrosis and apoptosis in cells (Lin and Yang, 2008).

The apoptotic pathways rely on signal-transduction systems using membrane-derived phospholipid precursors as second messengers. Thus, an important marker of apoptotic signalling in cells is the changes to cellular lipid which are mostly represented by absorbance at wavenumbers in the range 2800 - 3000 cm^{-1} in the IR spectrum of the cell (Liu et al., 2001; Zelig et al., 2009). *De novo* protein synthesis, the modification of existing proteins and the phosphorylation/activation of specific proteins, *e.g.*, p53, are important attributes of apoptosis and the cellular response of cells following exposure to DNA-damaging compounds (Hockley et al., 2007). Based on these, increased lipid absorbance, decreased DNA absorbance and an increase in the β -secondary structure of total cellular protein in the IR spectra could be regarded as biomarkers for apoptosis in cells. In this study, the high B[a]P concentration induced significant increases in proteins/lipids and decreased nucleic acids as well as phosphorylated protein. Furthermore, the relationship between lipids, proteins, nucleic acids and phosphorylated protein (Figs. 4 & 5) suggests the possible signalling of apoptosis in treated cells. Finally, significant correlation between the peak areas for intact cells and isolated nuclei may imply that the protein/DNA regions, as well as alterations to these regions in IR spectra of whole cells, may be a reflection of alterations in its nucleus.

5. Conclusion

There is much information in an IR spectrum of a biological sample (Trevisan et al., 2012). More interestingly, this information can be obtained almost reagent-free and with a relatively small amount of sample (Baker et al., 2014). Using ATR-FTIR spectroscopy, this study observed B[a]P-induced responses in whole cells and isolated nuclei of MCF-7 cells

concentrated in G₀/G₁- and S-phases. B[a]P induced dose-related responses and marked alterations within the DNA/RNA region of the biochemical cell fingerprint. Based on wavenumbers distinguishing isolated nuclei in treated cells from those of control cell populations, these changes are possibly due to alterations to nucleic acid bases and the possible disruption of base-pairing/stacking interactions in the nucleus.

B[a]P induced an increase in the total biomolecules in G₀/G₁-phase cell populations, indicating the possible activation of growth factor receptor signalling. Increased lipids, increased protein and decreased DNA, as well as changes to nuclear lipids indicate the possibility of apoptosis signalling in treated cells. Our results show that IR spectroscopy is able to distinguish between treated cell populations at subcellular levels, in this case the nucleus. The technique is sensitive to slight changes in the biological molecules of cells including changes induced by exposure to low chemical doses. It is possible to derive mechanistic insights based on alterations to various regions of the biochemical-cell fingerprint. It provides further evidence supporting the application of IR spectroscopy to easily identify cellular/subcellular responses to chemical insults.

ACKNOWLEDGEMENTS: BEO is a Faculty for the Future Fellow of the Schlumberger Foundation, an independent non-profit entity that supports science and technology education. Such Fellowships support female academics from developing and emerging countries for advanced graduate study.

References

- Arlt, V.M., Stiborová, M., Henderson, C.J., Thiemann, M., Frei, E., Aimová, D., Singh, R., Gamboa da Costa, G., Schmitz, O.J., Farmer, P.B., Wolf, C.R., Phillips, D.H., 2008. Metabolic activation of benzo[*a*]pyrene in vitro by hepatic cytochrome P450 contrasts with detoxification in vivo: experiments with hepatic cytochrome P450 reductase null mice. *Carcinogenesis* 29, 656-665.
- Baker, M.J., Trevisan, J., Bassan, P., Bhargava, R., Butler, H.J., Dorling, K.M., Fielden, P.R., Fogarty, S.W., Fullwood, N.J., Heys, K.A., Hughes, C., Lasch, P., Martin-Hirsch, P.L., Obinaju, B., Sockalingum, G.D., Sule-Suso, J., Strong, R.J., Walsh, M.J., Wood, B.R., Gardner, P., Martin, F.L., 2014. Using Fourier transform IR spectroscopy to analyze biological materials. *Nature Protocols* 9, 1771-1791.
- Balasubramanian, K., Mirnikjoo, B., Schroit, A.J., 2007. Regulated externalization of phosphatidylserine at the cell surface implications for apoptosis. *Journal of Biological Chemistry* 282, 18357-18364.
- Banyay, M., Sarkar, M., Gräslund, A., 2003. A library of IR bands of nucleic acids in solution. *Biophysical Chemistry* 104, 477-488.
- Cakmak, G., Togan, I., Severcan, F., 2006. 17 β -Estradiol induced compositional, structural and functional changes in rainbow trout liver, revealed by FT-IR spectroscopy: a comparative study with nonylphenol. *Aquatic Toxicology* 77, 53-63.
- Dovbeshko, G.I., Gridina, N.Y., Kruglova, E.B., Pashchuk, O.P., 2000. FTIR spectroscopy studies of nucleic acid damage. *Talanta* 53, 233-246.
- Gasparri, F., Muzio, M., 2003. Monitoring of apoptosis of HL60 cells by Fourier-transform infrared spectroscopy. *Biochemical Journal* 369, 239-248.
- Hammiche, A., German, M.J., Hewitt, R., Pollock, H.M., Martin, F.L., 2005. Monitoring cell cycle distributions in MCF-7 cells using near-field photothermal microspectroscopy. *Biophysical Journal* 3699-3706.
- Hamouchene, H., Arlt, V.M., Giddings, I., Phillips, D.H., 2011. Influence of cell cycle on responses of MCF-7 cells to benzo[*a*]pyrene. *BMC Genomics* 12, 333.
- Hockley, S., Arlt, V., Brewer, D., Giddings, I., Phillips, D., 2006. Time- and concentration-dependent changes in gene expression induced by benzo[*a*]pyrene in two human cell lines, MCF-7 and HepG2. *BMC Genomics* 7, 260.

Hockley, S.L., Arlt, V.M., Brewer, D., te Poele, R., Workman, P., Giddings, I., Phillips, D.H., 2007. AHR- and DNA-Damage-Mediated Gene Expression Responses Induced by Benzo[*a*]pyrene in Human Cell Lines. *Chemical Research in Toxicology* 20, 1797-1810.

Holton, S.E., Walsh, M.J., Bhargava, R., 2011. Subcellular localization of early biochemical transformations in cancer-activated fibroblasts using infrared spectroscopic imaging. *Analyst* 136, 2953-2958.

Irvine, R.F., 2003. Nuclear lipid signalling. *Nature Reviews Molecular Cell Biology* 4, 349-361.

Jiao, H., Allinson, S.L., Walsh, M.J., Hewitt, R., Cole, K.J., Phillips, D.H., Martin, F.L., 2007. Growth kinetics in MCF-7 cells modulate benzo[*a*]pyrene-induced *CYP1A1* up-regulation. *Mutagenesis* 22, 111-116.

Khan, Q.A., Dipple, A., 2000. Diverse chemical carcinogens fail to induce G1 arrest in MCF-7 cells. *Carcinogenesis* 21, 1611-1618.

Lasch, P., Pacifico, A., Diem, M., 2002. Spatially resolved IR microspectroscopy of single cells. *Biopolymers* 67, 335-338.

Ledeen, R.W., Wu, G., 2006. Sphingolipids of the nucleus and their role in nuclear signaling. *Biochimica et Biophysica Acta (BBA)-Molecular and Cell Biology of Lipids* 1761, 588-598.

Lin, T., Yang, M.S., 2008. Benzo[*a*]pyrene-induced necrosis in the HepG2 cells via PARP-1 activation and NAD⁺ depletion. *Toxicology* 245, 147-153.

Ling, C., Poulsen, P., Simonsson, S., Rönn, T., Holmkvist, J., Almgren, P., Hagert, P., Nilsson, E., Mabey, A.G., Nilsson, P., 2007. Genetic and epigenetic factors are associated with expression of respiratory chain component NDUF6 in human skeletal muscle. *The Journal of Clinical Investigation* 117, 3427-3435.

Lipiec, E., Bambery, K.R., Heraud, P., Kwiatek, W.M., McNaughton, D., Tobin, M.J., Vogel, C., Wood, B.R., 2014. Monitoring UVR induced damage in single cells and isolated nuclei using SR-FTIR microspectroscopy and 3D confocal Raman imaging. *Analyst* 139, 4200-4209.

Liu, K.-Z., Jia, L., Kelsey, S.M., Newland, A., Mantsch, H., 2001. Quantitative determination of apoptosis on leukemia cells by infrared spectroscopy. *Apoptosis* 6, 269-278.

Llabjani, V., Hoti, V., Pouran, H.M., Martin, F.L., Zhang, H., 2014. Bimodal responses of cells to trace elements: Insights into their mechanism of action using a biospectroscopy approach. *Chemosphere* 112, 377-384.

Malins, D.C., Anderson, K.M., Stegeman, J.J., Jaruga, P., Green, V.M., Gilman, N.K., Dizdaroglu, M., 2006. Biomarkers signal contaminant effects on the organs of English sole (*Parophrys vetulus*) from Puget Sound. *Environmental Health Perspectives* 114, 823.

Martin, F.L., German, M.J., Wit, E., Fearn, T., Ragavan, N., Pollock, H.M., 2007. Identifying variables responsible for clustering in discriminant analysis of data from infrared microspectroscopy of a biological sample. *Journal of Computational Biology* 14, 1176-1184.

Movasaghi, Z., Rehman, S., ur Rehman, D.I., 2008. Fourier transform infrared (FTIR) spectroscopy of biological tissues. *Applied Spectroscopy Reviews* 43, 134-179.

Obinaju, B.E., Martin, F.L., 2013. Novel biospectroscopy sensor technologies towards environmental health monitoring in urban environments. *Environmental Pollution* 183, 46-53.

Obinaju, B.E., Alaoma, A., Martin, F.L., 2014. Novel sensor technologies towards environmental health monitoring in urban environments: a case study in the Niger Delta (Nigeria). *Environmental Pollution* 192, 222-231.

Obinaju, B.E., Graf, C., Halsall, C., Martin, F.L., 2015. Linking biochemical perturbations in tissues of the African catfish to the presence of polycyclic aromatic hydrocarbons in Ovia River, Niger Delta region. *Environmental Pollution* 201, 42-49.

Pang, W., Li, J., Ahmadzai, A.A., Heppenstall, L., Llabjani, V., Trevisan, J., Qiu, X., Martin, F.L., 2012. Identification of benzo[*a*]pyrene-induced cell cycle-associated alterations in MCF-7 cells using infrared spectroscopy with computational analysis. *Toxicology* 298, 24 - 29.

Phillips, D.H., 1983. Fifty years of benzo[*a*]pyrene. *Nature* 303, 468-472.

Pijanka, J.K., Kohler, A., Yang, Y., Dumas, P., Chio-Srichan, S., Manfait, M., Sockalingum, G.D., Sulé-Suso, J., 2009. Spectroscopic signatures of single, isolated cancer cell nuclei using synchrotron infrared microscopy. *Analyst* 134, 1176-1181.

Severcan, F., Gorgulu, G., Gorgulu, S.T., Guray, T., 2005. Rapid monitoring of diabetes-induced lipid peroxidation by Fourier transform infrared spectroscopy: Evidence from rat liver microsomal membranes. *Analytical Biochemistry* 339, 36-40.

Stuart, B., 2005. Infrared Spectroscopy, Kirk-Othmer Encyclopedia of Chemical Technology. John Wiley & Sons, Inc.

Tannheimer, S., Barton, S., Ethier, S., Burchiel, S., 1997. Carcinogenic polycyclic aromatic hydrocarbons increase intracellular Ca²⁺ and cell proliferation in primary human mammary epithelial cells. *Carcinogenesis* 18, 1177-1182.

Tannheimer, S., Ethier, S., Caldwell, K., Burchiel, S., 1998. Benzo [*a*] pyrene-and TCDD-induced alterations in tyrosine phosphorylation and insulin-like growth factor signaling pathways in the MCF-10A human mammary epithelial cell line. *Carcinogenesis* 19, 1291-1297.

Trevisan, J., Angelov, P.P., Patel, I.I., Najand, G.M., Cheung, K.T., Llabjani, V., Pollock, H.M., Bruce, S.W., Pant, K., Carmichael, P.L., Scott, A.D., Martin, F.L., 2010. Syrian hamster embryo (SHE) assay (pH 6.7) coupled with infrared spectroscopy and chemometrics towards toxicological assessment. *Analyst* 135, 3266-3272.

Trevisan, J., Angelov, P.P., Carmichael, P.L., Scott, A.D., Martin, F.L., 2012. Extracting biological information with computational analysis of Fourier-transform infrared (FTIR) biospectroscopy datasets: current practices to future perspectives. *Analyst* 137, 3202-3215.

Trevisan, J., Angelov, P.P., Scott, A.D., Carmichael, P.L., Martin, F.L., 2012. IRootLab: a free and open-source MATLAB toolbox for vibrational biospectroscopy data analysis. *Bioinformatics* 29, 1095-1097.

Yakovchuk, P., Protozanova, E., Frank-Kamenetskii, M.D., 2006. Base-stacking and base-pairing contributions into thermal stability of the DNA double helix. *Nucleic Acids Research* 34, 564-574.

Zelig, U., Kapelushnik, J., Moreh, R., Mordechai, S., Nathan, I., 2009. Diagnosis of cell death by means of infrared spectroscopy. *Biophysical Journal* 97, 2107-2114.